Negative-Sequence Virtual Circuit Breaker in Islanded Inverter-Based Microgrids

Mojtaba Ghodrati, Ángel Borrell, Miguel Castilla, Jaume Miret, *Member, IEEE*, and Manel Velasco

***Abstract*—Unbalanced loads in islanded inverter-based microgrids induce voltage and current imbalances, posing significant challenges to the operation of critical equipment and sensitive loads. To address this issue, conventional circuit breakers, strategically placed between microgrids, play a key role in fault isolation during unbalanced conditions. However, they exhibit weaknesses in effectively addressing power quality issues, frequency variations, and power supply interruptions to specific loads. To solve these limitations, this article introduces the new concept of a negative-sequence virtual circuit breaker. Microgrid inverters are responsible for implementing this concept, which consists of eliminating negative-sequence voltages and currents at the point of-common-coupling between microgrids without altering positive-sequence voltages and currents. This last issue allows the entire electrical system to operate on a single frequency, guaranteeing the loads' supply. The compensators responsible for implementing the proposed concept are unilateral bandpass filters with complex coefficients. The primary advantage of these compensators over conventional integral compensators is their ability to offer plug-and-play operation. The effectiveness of the proposed concept has been verified through experimental tests in a laboratory setup.**

***Index Terms*—Islanded inverter-based microgrids, negative sequence imbalances, unbalanced loads, virtual circuit breaker.**

I. Introduction

THE growing importance of inverter-based microgrids lies in their ability to independently convert power from renewable energy sources into local power using inverters, reflecting advancements that efficiently integrate diverse distributed generation sources while maintaining superior power quality [1], [2]. In this scenario, unbalanced faults generate negative-sequence voltages and currents throughout the entire microgrid, which may affect the reliability and stability of the system [3], [4], [5]. Strategically located between microgrids, conventional circuit breakers act as key components that facilitate the isolation of specific sections during faults, preventing potential cascading failures and contributing to the resilience of the entire system [6], [7]. In inverter-based microgrids, strategic integration of circuit breakers is very important along with efforts to eliminate negative-sequence voltages and currents in some sensitive nodes of the power networks [8], [9], [10].

When an unbalanced load occurs in the system, the circuit breaker detects the imbalance and opens, leading to fluctuations in the system voltage and frequency [11], [12]. In this scenario, the challenge of voltage and frequency resynchronization has been investigated [13], [14], [15]. While Sharma et al. [16] addressed synchronization methods during circuit breaker activation, the persistence of transient disturbances in the system frequency remains. In [17], a novel resynchronization approach for islanded unbalanced active distribution networks is introduced, utilizing a synchro-circuit breaker coupled with a controllable circuit breaker. Under specific conditions, circuit breaker openings result in power supply interruptions to specific loads, impacting overall load distribution and causing damage to microgrid equipment [18], [19], [20]. Additionally, system frequency changes during unbalances can lead to polarization challenges associated with the directional element of protective relays [21]. The context of polarization is addressed in [22] and [23]. Hence, circuit breakers must be designed to avoid affecting frequency and power flow when opening [24]. The use of an insulated gate-triggered thyristor (IGTT) is proposed in [25] for solid-state circuit breaker (SSCB) applications, aiming to enhance power efficiency and reliability. However, existing SSCBs often experience high reverse voltage stress during fault interruptions. In [26], a new SSCB based on the IGTT with a field-stop layer (FS-IGTT) for dc microgrid protection is introduced, prioritizing fault interruption without reflecting current surges to sources or loads. While this proposed SSCB offers more robust breaking capability and higher power efficiency compared to existing circuit breakers, it does not address the issue of frequency synchronization. Previous works have focused on circuit breakers' operation to attain and sustain synchronization during imbalances. However, challenges persist in addressing frequency variations and power distribution, particularly in scenarios with multiple distributed energy resources contributing to power generation within each microgrid. Conversely, circuit breaker strategies alone may not be sufficient to address frequency differences in islanded microgrids and transient power sharing when circuit breakers open.

Manuscript received 23 February 2024; revised 29 April 2024 and 12 June 2024; accepted 28 June 2024. Date of publication 8 July 2024; date of current version 4 September 2024. This work was supported by the I+D+i PID2021-122835OB-C21 research project, financed by MCIN/AEI/10.13039/501000011033 and FEDER "Una manera de hacer Europa." Recommended for publication by Associate Editor S. Golestan. *(Corresponding author: Mojtaba Ghodrati.)*

Mojtaba Ghodrati, Miguel Castilla, and Jaume Miret are with the Department of Electronic Engineering, Universitat Politècnica de Catalunya, 08800 Vilanova i la Geltrú, Spain (e-mail: mojtaba.ghodrati@upc.edu; miquel.castilla@upc.edu; jaume.miret@upc.edu).

Ángel Borrell is with the Department of Electrical Engineering, Escola Salesiana de Sarrià, 08017 Barcelona, Spain (e-mail: aborrell@euss.es).

Manel Velasco is with the Department of Automatic Control, Universitat Politècnica de Catalunya, 08028 Barcelona, Spain (e-mail: manel.velasco@upc.edu).

Color versions of one or more figures in this article are available at https://doi.org/10.1109/TPEL.2024.3424676.

Digital Object Identifier 10.1109/TPEL.2024.3424676

This article introduces the new concept of a negative-sequence virtual circuit breaker, which is designed to prevent voltage and current imbalances, resulting from a fault in a microgrid, from propagating to the rest of the power system. This article makes a significant contribution to the field by defining this concept and demonstrating its implementation in the local controllers of the microgrid inverters. Advanced control algorithms enable the virtual circuit breaker to efficiently eliminate negative-sequence voltage at the point-of-common-coupling (PCC) between the microgrids. Notably, the virtual circuit breaker ensures the preservation of positive-sequence voltages and currents, allowing the system to operate seamlessly with a single frequency and powering the loads of all microgrids collectively and uninterruptedly. Furthermore, the compensators in the local controllers are unilateral bandpass filters with complex coefficients. The primary advantage of these compensators over conventional integral compensators is their ability to offer the interesting feature of plug-and-play operation. This innovative solution not only addresses the limitations of conventional circuit breakers but also optimizes energy distribution, enhances resilience, and safeguards sensitive loads within islanded microgrids.

The rest of this article is organized as follows. Section II introduces the system and formulates the problem. Section III presents the concept of a negative-sequence virtual circuit breaker and proposes a practical control scheme for the microgrid inverters. In Section IV, a dynamic model of the closed-loop system is presented. In Section V, a design procedure for the proposed control is presented. The virtual circuit breaker validity is shown in Section VI through experimental tests conducted in a laboratory microgrid. Finally, Section VII concludes this article.

II. System Description and Problem Formulation

This section includes variable definition, system description, and circuit breaker states. Finally, the problem is formulated.

A. Definition of Variables

This article considers complex-valued variables to compact notation. The complex-valued positive- and negative-sequence components are written as a function of real-valued stationary-reference frame variables as

$$x^{+}\ (t) = x_{\alpha}^{+}\ (t) + jx_{\beta}^{+}\,(t) \tag{1}$$

$$x^{-}\ (t) = x_{\alpha}^{-}\ (t) + jx_{\beta}^{-}\,(t)\,. \tag{2}$$

Complex-conjugate variables are useful for modeling system imbalances [27], [28], [29]. These variables can be written as

$$\overline{x^{+}}\ (t) = x_{\alpha}^{+}\ (t) - jx_{\beta}^{+}\,(t) \tag{3}$$

$$\overline{x^{-}}\ (t) = x_{\alpha}^{-}\ (t) - jx_{\beta}^{-}\,(t)\,. \tag{4}$$

Finally, the complex-valued variable $x(t)$ is expressed by combining positive- and negative-sequence components as

$$x\ (t) = x^{+}\ (t) + x^{-}\,(t)\,. \tag{5}$$

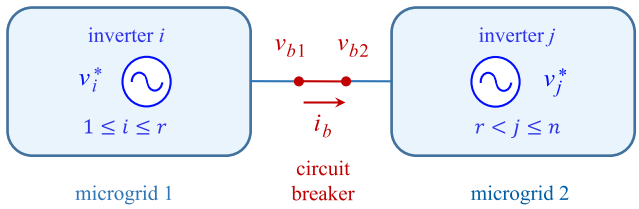

Fig. 1. Islanded power system with two inverter-based microgrids.

B. System Description

Fig. 1 shows the scheme of an islanded power system with two microgrids equipped with grid-forming inverters [30], [31]. Microgrids 1 and 2 include r and $n-r$ inverters, respectively, where n is the total number of grid-forming inverters in the power system. These grid-forming inverters are responsible for regulating their output voltage. This function is reached by programming an adequate reference voltage (see v_i^* and v_j^* in Fig. 1). The droop method [32], virtual synchronous generator [33], and virtual oscillator [34] are typical control algorithms used to program the reference voltages.

A circuit breaker is placed in between both microgrids. This element is essential to isolate faults within one of the microgrids, thus avoiding the disturbance propagating along the power system.

C. Circuit Breaker States

The circuit breaker in Fig. 1 has two states: closed or open. When the power system is in normal operation, the circuit breaker is closed. In this case, the circuit breaker voltage and current can be expressed as

$$v_{b1}\ (t) = v_{b2}\ (t) \tag{6}$$

$$i_b\,(t) \neq 0. \tag{7}$$

When there is a fault in one of the microgrids, the circuit breaker is open. In this case, the circuit breaker voltage and current can be written as

$$v_{b1}\,(t) \neq v_{b2}\,(t) \tag{8}$$

$$i_b\ (t) = 0 \tag{9}$$

D. Problem Statement

The problem to be solved in this article is to prevent the transmission of voltage and current imbalances from a faulted microgrid to the rest of the power system. Furthermore, it is desired to solve this problem by keeping the circuit breaker in Fig. 1 closed, with the intention of not causing frequency variations or interruptions in the power supply. Imbalance transmission is avoided by eliminating the negative-sequence current through the circuit breaker, which is hereafter referred to as control objective 1

$$i_{b,ss}^{-} = 0. \tag{10}$$

It should be noted that (6) is still satisfied, given that the circuit breaker is in the closed position.

In addition, imbalances should be prevented from being transmitted while improving power quality at PCC between microgrids. In steady state, this is referred to as control objective 2 and can be written as

$$\bar{v_{b1,ss}} = \bar{v_{b2,ss}} = 0. \tag{11}$$

Finally, the problem is fully stated by indicating that the balance between power generation and consumption must be maintained, which is called control objective 3. This is achieved by ensuring active power sharing among microgrid inverters

$$\frac{P_{i,ss}}{S_{\text{rated},i}} = \frac{P_{i+1,ss}}{S_{\text{rated},i+1}} \tag{12}$$

where $P_{i,ss}$ and $S_{\text{rated},i}$ are the steady-state active power and rated power of inverter i (for $i = 1, \ldots, n-1$).

III. Proposed Solution

This section introduces the new concept of a negative-sequence virtual circuit breaker and proposes a control scheme to implement it in practice.

A. Negative-Sequence Virtual Circuit Breaker

The negative-sequence virtual circuit breaker is a new control concept that prevents the transmission of voltage and current imbalances through the power system. To implement this concept, the control system of the microgrid inverters must be augmented with a negative-sequence control scheme that achieves control objectives 1 and 2.

It is worth noting that the virtual circuit breaker is applied to a conventional circuit breaker in a closed state. In other words, the circuit breaker must be kept closed between the microgrids, whereas the inverters are operating to achieve control objectives 1 and 2. Although the circuit breaker is always closed, it is essential to maintain it in situations where it is necessary to electrically isolate a portion of the power system (e.g., for maintenance or equipment replacement).

To conclude the description of the virtual circuit breaker concept, it is important to note that control objectives 1 and 2 should be achieved with a negative-sequence controller that should not have significant interactions with the controller responsible for achieving control objective 3.

B. Control Requirements

To achieve control objectives 1 and 2, $v_b(t)$ and $i_b(t)$ must be remotely sensed and sent to the inverters through a communication system (see Fig. 2). In this figure, $v_b(t)$ denotes the circuit breaker voltage (subscripts 1 or 2 are not necessary for this variable since the physical circuit breaker is always closed). Note that $v_b(t)$ and $i_b(t)$ are inputs to the local control scheme of each inverter, which is responsible for achieving compliance with (10) and (11). Control objective 3 is achieved by the droop method, which is a conventional control method that uses only locally sensed variables [32]. This is a particular choice in this article although other power-sharing methods could be used [33], [34].

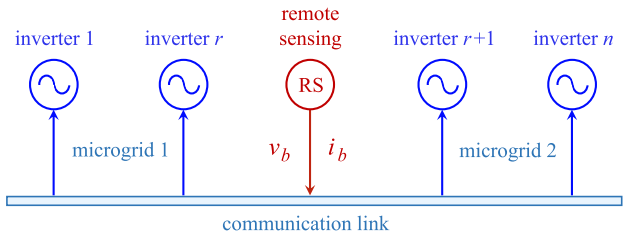

Fig. 2. Communication system.

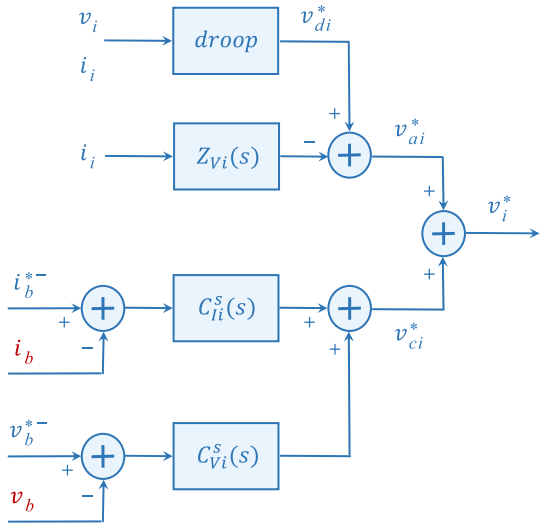

Fig. 3. Control scheme for inverter i.

C. Proposed Control Scheme for Inverter i

Fig. 3 shows the diagram of the proposed control scheme for inverter i. At the top of this figure, the droop method is augmented with a virtual impedance to guarantee controllability in microgrids with resistive, inductive, and mixed grid impedances [35], [36]

$$v_{ai}^*(s) = v_{di}^*(s) - Z_{Vi}(s)\, i_i(s) \tag{13}$$

where v_{di}^* is the output voltage of the droop method [32] and Z_{Vi} the virtual impedance [35].

At the bottom of the figure, the compensators $C_{Ii}^s(s)$ and $C_{Vi}^s(s)$ implement the virtual circuit breaker concept. In fact, they are in charge of processing the negative-sequence component of current and voltage in the circuit breaker, respectively. The selection of these compensators is a key aspect of the proposed control. To avoid cross-coupling interactions between both control variables, it is preferred to dedicate one of the microgrids to negative-sequence current compensation and the other to negative-sequence voltage compensation. This choice is based on the analysis of cross-coupling interactions using the relative gain array method. For the interested reader, some examples of the application of this method can be found in [37] and [38].

Therefore, in the microgrid inverters responsible for current compensation, the compensator $C_{Vi}^s(s) = 0$. Similarly, in the microgrid inverters responsible for voltage compensation the

TABLE I
CURRENT AND VOLTAGE COMPENSATORS

Microgrid	$C_{Ii}^{s}(s)$	$C_{Vi}^{s}(s)$
1	$\frac{k_{Ii}2\xi_{Ii}\omega_0}{s+2\xi_{Ii}\omega_0+j\omega_0}$	0
2	0	$\frac{k_{Vi}2\xi_{Vi}\omega_0}{s+2\xi_{Vi}\omega_0+j\omega_0}$

compensator $C_{Ii}^{s}(s)=0$. In this article, the assignment of current and voltage compensation is given as follows.

1) Inverters in microgrid 1 perform current compensation to achieve the control objective (10).
2) Inverters in microgrid 2 perform voltage compensation to accomplish the control objective (12).

The compensators shown in Table I guarantee the desired features. Note that the compensators are unilateral bandpass filters with complex coefficients [39], [40]. The control parameters $k_{Ii}, k_{Vi} \in \mathbb{C}$ are the gains of the compensators evaluated at the frequency $s=-j\omega_0$, whereas $\xi_{Ii}, \xi_{Vi} \in \Re$ are the damping factors of the compensators. To reach the control objectives 1 and 2, the reference signals must be chosen as $i_b^{*-}=0$ and $v_b^{*-}=0$, respectively.

D. Standard Control as a Basis for Comparison

Focusing on complex-valued compensators, the standard control is an integral term with complex coefficients

$$C(s)=\frac{k}{s+j\omega_0} \tag{14}$$

where k is the integral gain. The gain of this compensator is ∞ at $s=-j\omega_0$, so it completely eliminates negative-sequence errors. This solution is an excellent choice in applications where each inverter is responsible for meeting a control objective without the collaboration of other inverters. For example, this is the case in a stand-alone inverter responsible for suppressing the negative-sequence voltage at its local output [41], [42]. However, it is not a suitable option to implement the virtual circuit breaker, since in this application several inverters work together in collaboration to achieve control objectives 1 and 2. The primary disadvantage of the integral compensator is its lack of plug-and-play functionality. In other words, when the system is operating in a steady state and the control objectives have already been achieved, it is not possible to incorporate additional inverters into the collaborative operation. This phenomenon can be attributed to the fact that the error to be corrected is zero and the output of the new integral is also zero.

The mentioned issue does not arise in the compensators shown in Table I, as their gain is finite at the frequency $s=-j\omega_0$. Consequently, these compensators introduce a small error that allows them to provide plug-and-play operation. Through the proper design of the compensator gains, these errors can be made negligible in practice. A suitable control design procedure to achieve this goal is presented in Section V.

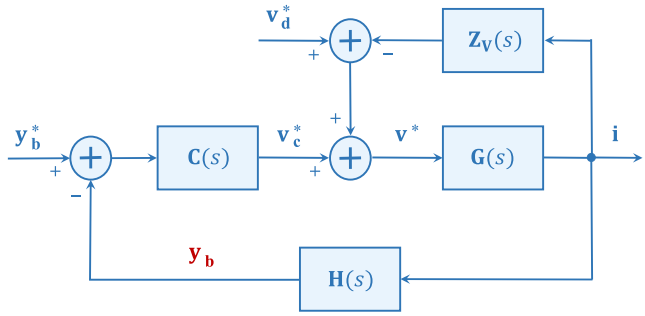

Fig. 4. Diagram of the closed-loop system.

IV. DYNAMIC MODEL OF THE CLOSED-LOOP SYSTEM

This section presents the dynamic model of the closed-loop system shown in Fig. 4. This is a large-signal linear model that describes the behavior of the complete power system shown in Fig. 1.

A. Definition of Vector Variables

In Fig. 4, variables $\mathbf{i}(s)$, $\mathbf{v}^*(s)$, $\mathbf{v_d^*}(s)$, and $\mathbf{v_c^*}(s)$ contain information about all inverters (1 to n), whereas $\mathbf{y_b}(s)$ contains information about the circuit breaker. Their components include positive- and negative-sequence variables and their complex conjugates. In general form, they can be written as

$$\mathbf{x}(s)=\left[x_1^+(s)\ \ldots\ x_n^+(s)\ x_1^-(s)\ \ldots\ x_n^-(s)\ \overline{x_1^+}(s)\ \ldots\ \overline{x_n^+}(s)\ \overline{x_1^-}(s)\ \ldots\ \overline{x_n^-}(s)\right]^T \in \mathbb{C}^{4n\text{x}1} \tag{15}$$

$$\mathbf{y_b}(s)=\left[i_b^+(s)\ v_b^+(s)\ i_b^-(s)\ v_b^-(s)\ \overline{i_b^+}(s)\ \overline{v_b^+}(s)\ \overline{i_b^-}(s)\ \overline{v_b^-}(s)\right]^T \in \mathbb{C}^{8\text{x}1} \tag{16}$$

where $\mathbf{x}(s)$ is valid for $\mathbf{i}(s)$, $\mathbf{v}^*(s)$, $\mathbf{v_d^*}(s)$, and $\mathbf{v_c^*}(s)$. The variable $\mathbf{y_b^*}(s)$ has the same structure than $\mathbf{y_b}(s)$, but its components include the superscript $*$.

B. Open Loop Model

The open loop model of the islanded microgrid in Fig. 1 can be written as

$$\mathbf{i}(s)=\mathbf{G}(s)\,\mathbf{v}^*(s) \tag{17}$$

$$\mathbf{y_b}(s)=\mathbf{H}(s)\,\mathbf{i}(s) \tag{18}$$

where the matrices $\mathbf{G}(s)$ and $\mathbf{H}(s)$ can be expressed as

$$\mathbf{G}(s)=\begin{bmatrix}\mathbf{G^s}(s) & 0 & 0 & \mathbf{G^a}(s)\\ 0 & \mathbf{G^s}(s) & \mathbf{G^a}(s) & 0\\ 0 & \overline{\mathbf{G^a}}(s) & \overline{\mathbf{G^s}}(s) & 0\\ \overline{\mathbf{G^a}}(s) & 0 & 0 & \overline{\mathbf{G^s}}(s)\end{bmatrix} \in \mathbb{C}^{4n\times 4n} \tag{19}$$

$$\mathbf{H}\ (s) = \begin{bmatrix} \mathbf{H^s}\,(s) & 0 & 0 & \mathbf{H^a}\,(s) \\ 0 & \mathbf{H^s}\,(s) & \mathbf{H^a}\,(s) & 0 \\ 0 & \overline{\mathbf{H^a}}\,(s) & \overline{\mathbf{H^s}}\,(s) & 0 \\ \overline{\mathbf{H^a}}\,(s) & 0 & 0 & \overline{\mathbf{H^s}}\,(s) \end{bmatrix} \in \mathbb{C}^{8\times 4n}. \tag{20}$$

The elements of $\mathbf{G^s}(s)$, $\mathbf{G^a}(s)$, $\mathbf{H^s}(s)$, and $\mathbf{H^a}(s)$ are obtained from Fig. 1 by applying: modified nodal analysis [43], Clarke transformation, and, the complexification expressed in (1)–(4).

C. Control Model

The complete control system can be obtained by grouping the control in Fig. 3 for each of the inverters in Fig. 1. The dynamic model can be written as

$$\mathbf{v}^*\ (s) = \mathbf{v_d^*}\ (s) - \mathbf{Z_v}\,(s)\,\mathbf{i}\,(s) + \mathbf{v_c^*}\,(s) \tag{21}$$

$$\mathbf{v_c^*}\ (s) = \mathbf{C}\,(s)\,(\mathbf{y_b^*}\,(s) - \mathbf{y_b}\,(s)) \tag{22}$$

where

$$\mathbf{Z_v}\ (\mathrm{s}) = \begin{bmatrix} \mathbf{Z_v^s}\,(\mathrm{s}) & \mathbf{0} & \mathbf{0} & \mathbf{0} \\ \mathbf{0} & \mathbf{Z_v^s}\,(\mathrm{s}) & \mathbf{0} & \mathbf{0} \\ \mathbf{0} & \mathbf{0} & \overline{\mathbf{Z_v^s}}\,(\mathrm{s}) & \mathbf{0} \\ \mathbf{0} & \mathbf{0} & \mathbf{0} & \overline{\mathbf{Z_v^s}}\,(\mathrm{s}) \end{bmatrix} \in \mathbb{C}^{4n\times 4n} \tag{23}$$

$$\mathbf{Z_v^s}\ (\mathbf{s}) = \begin{bmatrix} Z_v\,(s) & 0 & \dots & 0 \\ 0 & Z_v\,(s) & \dots & 0 \\ \dots & \dots & \dots & \dots \\ 0 & 0 & \dots & Z_v\,(s) \end{bmatrix} \in \mathbb{C}^{n\times n} \tag{24}$$

$$\mathbf{C}\ (\mathrm{s}) = \begin{bmatrix} \mathbf{0} & \mathbf{0} & \mathbf{0} & \mathbf{0} \\ \mathbf{0} & \mathbf{C^s}\,(\mathrm{s}) & \mathbf{0} & \mathbf{0} \\ \mathbf{0} & \mathbf{0} & \mathbf{0} & \mathbf{0} \\ \mathbf{0} & \mathbf{0} & \mathbf{0} & \overline{\mathbf{C^s}}\,(\mathrm{s}) \end{bmatrix} \in \mathbb{C}^{4n\times 8} \tag{25}$$

$$\mathbf{C^s}\ (\mathbf{s}) = \begin{bmatrix} C_{I1}^s\,(s) & 0 \\ \dots & \dots \\ C_{Ir}^s\,(s) & 0 \\ 0 & C_{Vr+1}^s\,(s) \\ \dots & \dots \\ 0 & C_{Vn}^s\,(s) \end{bmatrix} \in \mathbb{C}^{n\times 2}. \tag{26}$$

D. Closed-Loop Model

The closed-loop model is obtained using (17), (18), (21), and (22). Considering that $\mathbf{y_b^*}\ (s) = 0$ to reach control objectives 1 and 2, the closed-loop model can be expressed as

$$\mathbf{i}\ (\mathrm{s}) = (\mathbf{I} + \mathbf{L}\,(\mathrm{s}))^{-1}\ \mathbf{G}\,(\mathrm{s})\,\mathbf{v_d^*}\,(\mathrm{s}) \tag{27}$$

where the loop gain $\mathbf{L}(\mathrm{s}) \in \mathbb{C}^{4n\times 4n}$ is written as

$$\mathbf{L}\ (\mathrm{s}) = \mathbf{G}\,(\mathrm{s})\,(\mathbf{Z_v}\,(\mathrm{s}) + \mathbf{C}\,(\mathrm{s})\,\mathbf{H}\,(\mathrm{s}))\,. \tag{28}$$

V. Control Design

This section presents a design procedure for the negative-sequence control shown in Fig. 3. It is based on the static and dynamic conditions derived in the following.

A. Steady-State Analysis

The fulfillment of control objectives 1 and 2 is theoretically validated by evaluating the closed-loop model at the frequency $s = -j\omega_0$ (i.e., the frequency of the negative-sequence components). By inserting (27) in (18), the circuit breaker variable in steady-state $\mathbf{y_{b,ss}}$ can be written as

$$\mathbf{y_{b,ss}} = \mathbf{H}\,(-j\omega_0)\,(\mathbf{I} + \mathbf{L}\,(-j\omega_0))^{-1}\mathbf{G}\,(-j\omega_0)\,\mathbf{v_{d,ss}^*} \tag{29}$$

where the loop gain is

$$\mathbf{L}\ (-j\omega_0) = \mathbf{G}\,(-j\omega_0)\,(\mathbf{Z_v}\,(-j\omega_0) + \mathbf{C}\,(-j\omega_0)\,\mathbf{H}\,(-j\omega_0))\,. \tag{30}$$

As discussed above, the negative-sequence components of $\mathbf{y_{b,ss}}$ (i.e., $\mathbf{y_{b,ss}^-}$) cannot be completely $\mathbf{0}$ in practice due to the finite gain of the compensators in Table I. The practical consequence of this fact is negligible if the following static condition is achieved by design

$$\mathbf{y_{b,ss}^-} \leq \mathbf{y_{b,max}^-} \tag{31}$$

provided that the specification $\mathbf{y_{b,max}^-}$ is chosen sufficiently small.

B. Stability Analysis

The stability analysis is based on the generalized Nyquist criterion [44]. The closed-loop system in (27) is guaranteed to be asymptotically stable if the Nyquist curves of the eigenvalues of $\mathbf{L}(j\omega)$ in (28) avoid encirclements of $-1 + j\,0$. In fact, each of the $4n$ eigenvalues (obtained from the square matrix $\mathbf{L}$ of order $4n$) must satisfy this condition. Note that the closed-loop system is a large-signal linear model. Therefore, the stability results have large signal validity.

C. Design Procedure

The step-by-step procedure for designing the control gains of the compensators in Table I is as follows.

1) Find a range of possible solutions from the steady-state analysis in (29)–(31).
2) Select a particular solution within the range and assess the dynamic specifications, including the stability of the system using the Nyquist criterion.
3) If the system is unstable, return to step 1 and relax the static specification by increasing the value of $\mathbf{y_{b,max}^-}$.
4) Repeat the above step until the system is stable.

VI. Experimental Validation

This section validates the performance of the proposed control through experiments conducted in a laboratory setup.

A. Laboratory Setup

Fig. 5 shows the laboratory setup, including five grid-forming inverters distributed across two microgrids which are interconnected by a circuit breaker. Loads 1 and 2 (labeled *L*1 and *L*2 in the figure) are balanced, and load 3 (*L*3) is unbalanced. Table II lists the nominal values of the microgrid components. With regard to the design of the standard droop method and virtual

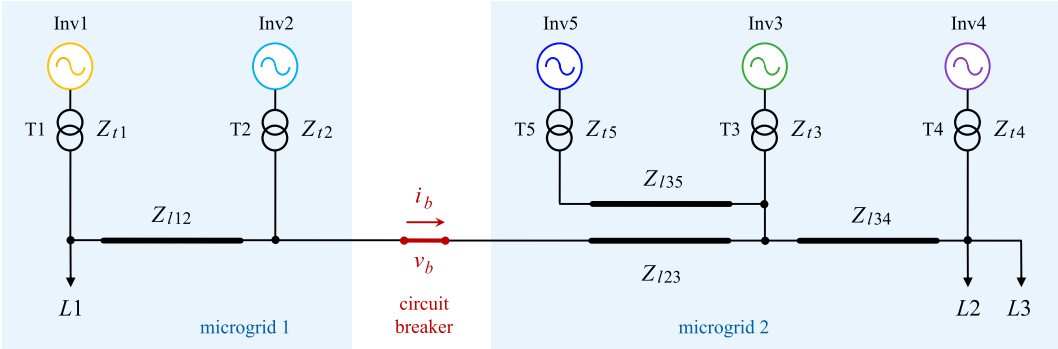

Fig. 5. Laboratory setup (the color of the circuit breaker and inverters is used to identify their experimental waveforms in Figs. 8, 9, and 11).

TABLE II
NOMINAL VALUES OF THE LABORATORY MICROGRID

Description	Symbol	Nominal value
Inverter rated power	$S_{rated,i}$	2.3 kVA
Inverter rated voltage	V_{oi}	155 V (peak)
Inverter rated current	$I_{rated.i}$	10 A (peak)
Switching and sampling freq.	f_{si}	10 kHz
Measuring unit transmission freq.	f_{ti}	10 Hz
Microgrid angular frequency	ω_o	$2\pi 60$ rad/s
Transformer impedances	Z_{t1}, Z_{t2}	$0.5 + j\,0.4\ \Omega$
Transformer impedances	Z_{t3}, Z_{t4}, Z_{t5}	$1.1 + j\,0.2\ \Omega$
Power line impedances	Z_{l12}, Z_{l35}	$j\,0.8\ \Omega$
Power line impedances	Z_{l23}, Z_{l34}	$j\,0.3\ \Omega$
Load 1: balanced	$L1$	1 kW
Load 2: balanced	$L2$	1.5 kW
Load 3: unbalanced	$L3$	2.5 kW
Active power droop coefficient	$m_{i,P}$	0.3 rad/(s kW)
Reactive power droop coefficient	$m_{i,Q}$	0.05 V/kVAr
Virtual inductance	$L_{i,V}$	8 mH

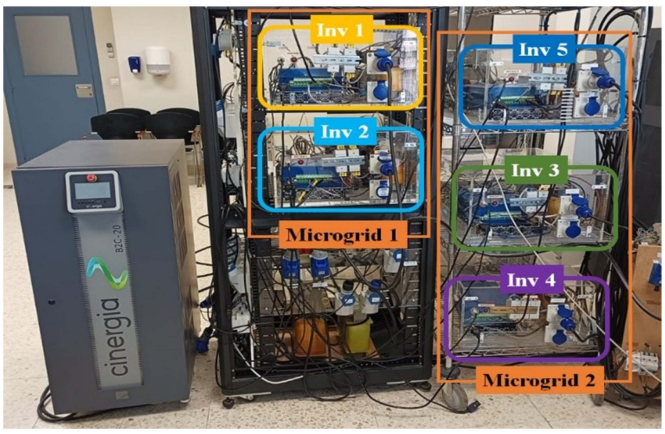

Fig. 6. Laboratory setup.

impedance gains in Table II, the reader is referred to [32], [35], and [36].

Fig. 6 shows a photograph of the laboratory setup, including the two microgrids and a Cinergia B2C-20 dc power supply used as the input source of the inverters. In this setup, the virtual circuit breaker concept is programmed in the control board of all inverters, which is based on a Texas Instruments F28M36 Concerto dual-core microcontroller. All the control boards are connected to a hub card using an Ethernet link. The remote sensing unit, implemented with the same control board, transmits v_b and i_b through the Ethernet link. The signals of interest are exported to MATLAB to represent the results. The following sections present the amplitudes of the ac voltages and currents (these dc variables are shown in capital letters), which are obtained using the sequence extractor presented in [45]. It is worth mentioning that this signal processor algorithm exhibits low-pass filter characteristics for the amplitudes [46]. The transient response of these signals facilitates the observation of compliance with control objectives 1 and 2.

TABLE III
SPECIFICATIONS OF THE CONTROL DESIGN

Description	Symbol	Nominal value
Maximum value for V_b^-	$V_{b,max}^-$	100 mV
Maximum value for I_b^-	$I_{b,max}^-$	50 mA
Maximum settling time for V_b^-	$t_{s,V,max}$	5 s
Maximum settling time for I_b^-	$t_{s,I,max}$	5 s
Maximum overshoot for V_b^-	$\Delta V_{b,max}^-$	0 %
Maximum overshoot for I_b^-	$\Delta I_{b,max}^-$	0 %

B. Design of the Proposed Control

The gains of the proposed control have been designed using the procedure presented in Section V-C. The control design starts with the definition of the static specifications of the proposed control, as detailed in Table III. Thereafter, a set of design constraints for the control gains is obtained by inserting the nominal values of the laboratory microgrid in (29)–(31). These constraints can be expressed for the considered microgrid as follows:

$$|k_{Ii}| < 557.8\ \Omega \tag{32}$$

$$\xi_{Ii} < 60.5\ 10^{-6} \tag{33}$$

$$|k_{Vi}| < 968.1\ \Omega \tag{34}$$

TABLE IV
DESIGN SOLUTION TO THE PROPOSED CONTROL

Description	Symbol	Nominal value
Control gain (MG1: $1 \leq i \leq r$)	k_{Ii}	$160 - j60\ \Omega$
Damping factor (MG1: $1 \leq i \leq r$)	ξ_{Ii}	$11.2\ 10^{-6}$
Control gain (MG2: $r < i \leq n$)	k_{Vi}	$160 + j60$
Damping factor (MG2: $r < i \leq n$)	ξ_{Vi}	$37.1\ 10^{-6}$

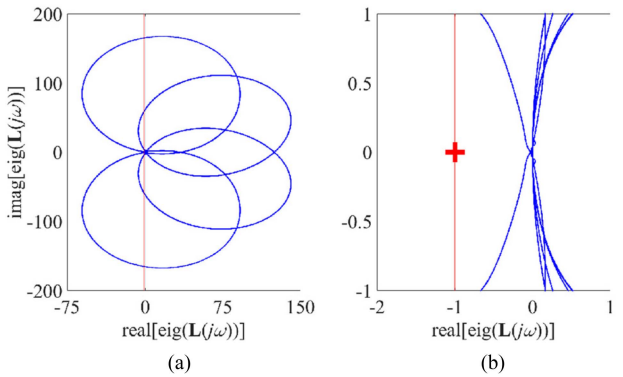

Fig. 7. Nyquist curves of the eigenvalues of $\boldsymbol{L}(j\omega)$. (a) Full plot. (b) Zoom-in of the full plot near the critical point $-1 + j0$.

$$\xi_{Vi} < 276.9\ 10^{-6}. \tag{35}$$

Table IV presents the proposed solution to this design problem, in which the control gains fulfill the constraints (32)–(35). It should be noted that the control solution includes the appropriate angle of the complex-valued gains k_{Ii} and k_{Vi}. This solution satisfies the dynamic specifications in Table III and is asymptotically stable. This last fact is shown in Fig. 7, in which the 20 eigenvalues of $\mathbf{L}$ avoid encircling the point $-1 + j0$.

C. Design of the Tests

The performance of the proposed virtual circuit breaker concept is validated by two experimental tests. Table V lists the conditions of the two tests. It should be noted that in both tests, the droop method and the virtual impedance controllers (see Fig. 3) are always active. Thus, the state of the virtual circuit breaker refers only to the negative-sequence control.

The tests start at $t = 0$ s, with the inverters in steady-state supplying the balanced loads 1 and 2 (2.5 kW total) and with the circuit breaker closed. At $t = 5$ s, the unbalanced load 3 (2.5 kW) is switched ON. At $t = 10$ s, the scenario of the two tests diverges. In test 1, the circuit breaker is triggered when the fault is detected. This occurs when the integral of the negative-sequence current amplitude I_b^- exceeds a set point. It is important to note that the control implementing the virtual circuit breaker concept is disabled in this test. In test 2, the circuit breaker remains closed for the entire duration. This is achieved by selecting a higher set point for triggering. In this test, the virtual circuit breaker is enabled at $t = 10$ s.

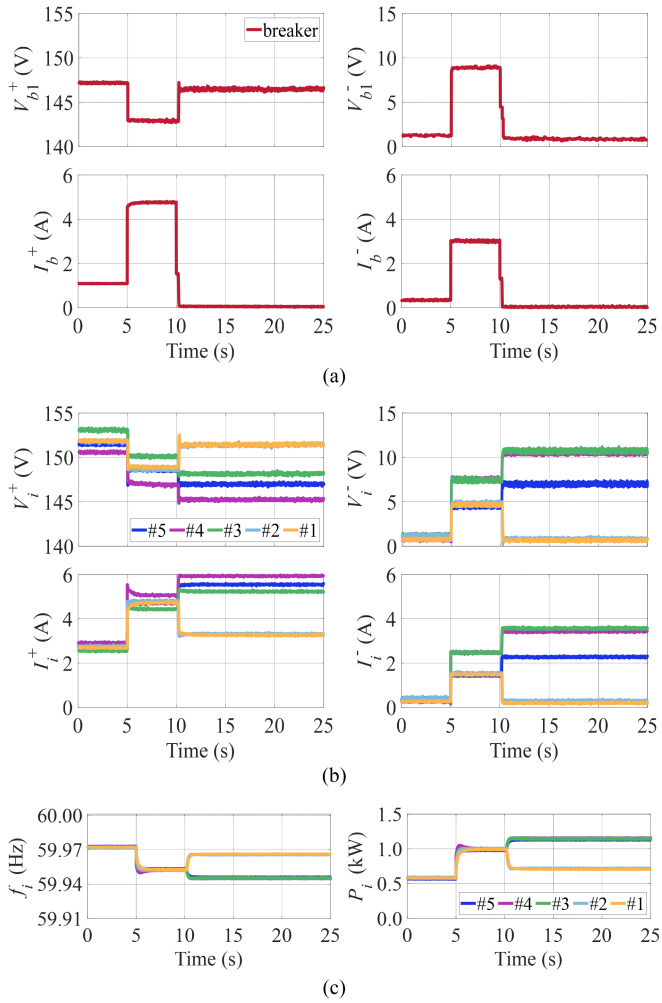

Fig. 8. Experimental results for test 1. Sequence components of the voltage and current amplitudes in (a) circuit breaker, (b) inverters, and (c) inverter frequencies and active powers.

The following is a performance comparison between the two tests. The signals of interest in this comparison are the amplitudes of the voltage and current sequence components in the circuit breaker and inverters and the frequency and the active power of each inverter.

D. Experimental Results for Test 1

Fig. 8 shows the signals of interest for test 1. In the first interval, the balanced load is jointly supplied by the five inverters with a positive-sequence current amplitude I_i^+ of 2.2 A [see Fig. 8(b)]. In this interval, the negative-sequence current amplitude I_i^- is about 0.3 A showing that the system is practically balanced. In the circuit breaker, there is a positive-sequence current of $I_b^+ = 1.1$ A flowing from microgrid 2 to microgrid 1 due to the power balance in the system [see Fig. 8(a)]. Finally, all inverters deliver the same active power $P_i = 520$ W and operate at the same frequency $P_i = 59.97$ Hz [see Fig. 8(c)]. Note that a steady-state error is observed at the inverter frequencies (nominal value is 60 Hz) due to the droop method being used.

TABLE V
CONDITIONS OF THE EXPERIMENTAL TESTS

Scenario		Test 1		Test 2	
Interval	Loads	Circuit breaker	Virtual circuit breaker	Circuit breaker	Virtual circuit breaker
$t \leq 5$ s	Balanced	Closed	Disabled	Closed	Disabled
5 s $< t \leq 10$ s	Unbalanced	Closed	Disabled	Closed	Disabled
$t > 10$ s	Unbalanced	Open	Disabled	Closed	Enabled

In the second interval, the unbalanced load is switched on. This causes an increase in both positive- and negative-sequence currents. In the inverters, the current I_i^+ almost doubles when the total load changes from 2.5 to 5 kW [see Fig. 8(b)]. Since the unbalanced load is connected to microgrid 2 ($L3$), the inverters of this microgrid have higher negative-sequence voltage ($V_i^- = 7.8$ V) than the inverters of microgrid 1 ($V_i^- = 4.6$ V). This is also true for the currents: $I_i^- = 2.2$ A for the inverters of microgrid 2 and $I_i^- = 1.3$ A for the inverters of microgrid 1. This effect is caused by the proximity to the disturbance, which in electrical terms is measured as the impedance that exists from the location of the inverters to the point where the disturbance occurs. As in the case of the inverters, the negative-sequence voltage and current in the circuit breaker also increase significantly with the connection of the unbalanced load [see Fig. 8(c)]. The main problem to be solved in this article is the elimination of the current I_b^-, which is 3.2 A in this interval. Eliminating this current prevents the propagation of the unbalance disturbance to the balanced microgrid. Finally, in Fig. 8(c), it is clear that the active power doubles when the load doubles, while the inverter frequencies decrease to 59.94 Hz. All inverters have the same operating point with a higher frequency error in steady-state.

In the third interval, the circuit breaker is open and the microgrids are electrically isolated. As a result, the current $I_b^- = 0$, as desired [see Fig. 8(a)]. The current I_b^+ is also 0. Focusing on the inverter currents, the inverters of microgrid 1 provide $I_i^- = 0$ (desired situation), whereas the unbalanced load is fully supplied by the inverters of microgrid 2 [see Fig. 8(b)]. In addition, the microgrids operate at different frequencies, and the inverters of each microgrid supply its local loads [see Fig. 8(c)].

E. Experimental Results for Test 2

Fig. 9 shows the main experimental results for test 2. The waveforms in the first and second intervals coincide with those in test 1 because they were measured under the same conditions.

In the third interval, the circuit breaker remains closed and the virtual circuit breaker control is activated in the five inverters. As a result, the positive-sequence voltage and current in the circuit breaker and in all the inverters remain at the same values as those obtained in the second interval [see Fig. 9(a) and (b)]. In addition, all the inverters deliver the same active power and have the same operating frequency [see Fig. 9(c)]. Therefore, all loads are jointly supplied by all inverters. By focusing on the negative-sequence waveforms, it can be observed that the circuit breaker voltage and current are nearly eliminated [see Fig. 9(a)]. In fact, the measured steady-state results are $I_b^- = 29.5$ mA and $V_b^- = 81.4$ mV. Therefore, from a practical point of view, control objectives 1 and 2 are met. Fig. 10 presents oscilloscope waveforms that corroborate the results presented in Fig. 9(a). Furthermore, the measured settling times and overshoots are $t_{s,V} = 2.2$ s, $t_{s,I} = 4.9$ s, $\Delta V_b^- = 0\%$, and $\Delta I_b^- = 0\%$, which align perfectly with the dynamic specifications detailed in Table III. Finally, it should be noted that the unbalance disturbance does not propagate to microgrid 1, since the currents I_i^- in the inverters of this microgrid are reduced to the values before the disturbance; compare the first and third intervals in Fig. 9(b).

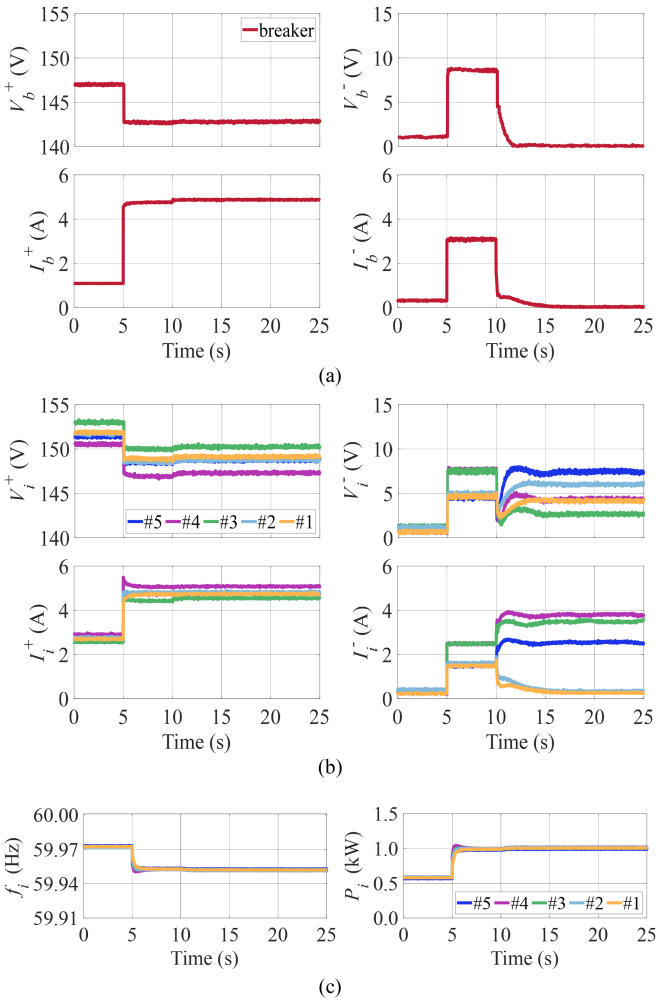

Fig. 9. Experimental results for test 2. Sequence components of the voltage and current amplitudes in (a) circuit breaker, (b) inverters, and (c) inverter frequencies and active powers.

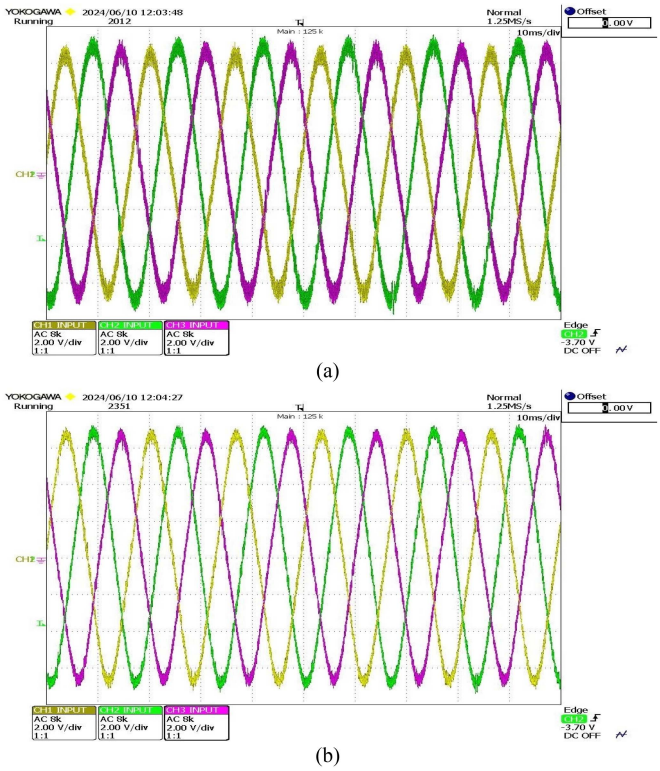

Fig. 10. Several periods of the phase voltages (45 V/div, 10 ms/div) at the circuit breaker during the intervals (a) $5\,\text{s} < t \leq 10\,\text{s}$ and (b) $t > 10\ s$.

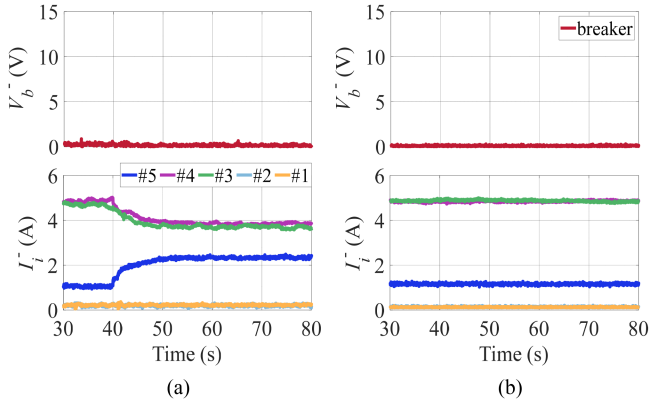

Fig. 11. Negative-sequence amplitudes in the circuit breaker voltage and inverter currents for test 2 with (a) compensators in Table I and (b) integral compensators in (14).

As a final remark, it should be noted that control objective 3 is met during the entire duration of the test, as illustrated in Fig. 9(c). This is due to the continuous operation of the droop method and virtual impedance controller throughout the test.

F. Discussion on the Results in Figs. 8–10

Looking at the results in Fig. 9, it is clear that the proposed control satisfactorily meets control objectives 1, 2, and 3. In fact, the imbalance fault is isolated and the power flow between the two microgrids is not interrupted using the novel virtual circuit breaker presented in this article. In addition to these essential features, this subsection discusses other relevant aspects of the proposal.

Inverters implementing the virtual circuit breaker concept should not be sized in any particular way. This fact can be seen in the negative-sequence currents delivered by the inverters in Fig. 9(b), third interval. Note that they have values very close to those measured in Fig. 8(b), third interval, when the virtual circuit breaker is disabled. Therefore, the use of an open circuit breaker or a virtual circuit breaker produces practically the same negative-sequence currents.

Using the same argument as in the previous paragraph, it can be stated that the efficiency of a system using a virtual circuit breaker is very similar to that of a system using a conventional circuit breaker. In other words, the use of the virtual circuit breaker does not penalize the sizing of the inverters or the efficiency of the power system. This is because the unbalanced load must be always supplied. In the virtual circuit breaker, this supply is carried out with an action of the inverters that also allows the elimination of the negative-sequence voltage and current in the circuit breaker.

G. Performance Comparison Between Compensators

This subsection validates the plug-and-play functionality of the compensators in Table I. To this end, test 2 was repeated with all five inverters in operation, but the proposed control was disabled in inverter 5 until $t = 30\,\text{s}$. Fig. 11(a) presents the results of this new test. As illustrated, the current in inverter 5 increases when its negative-sequence control is activated, enabling inverters 3 and 4 to reduce their current in this collaborative operation. This results in the achievement of the same steady-state values of initial test 2 (see Fig. 9). Regardless of whether the control in inverter 5 is enabled or disabled, the negative-sequence voltage at the circuit breaker remains practically zero, which substantiates the fulfillment of control objective 2.

It is noteworthy that in the aforementioned scenario, once the system reaches a steady state, the integral control does not permit the inverter 5 to participate in the elimination of the negative-sequence voltage at the circuit breaker. This phenomenon is illustrated in Fig. 11(b). The control of inverter 5 is enabled at $t = 30\,\text{s}$, yet in this instance, the currents do not undergo a change in value.

VII. Conclusion

In this article, the new concept of a negative-sequence virtual circuit breaker has been introduced. It consists of eliminating negative-sequence voltages and currents at the PCC between microgrids while maintaining system frequency and power sharing. To program the virtual circuit breaker, a control scheme has been presented for microgrid inverters. Furthermore, a theoretical framework to design the proposed control has also been presented. The proposal has been validated through extensive experiments in a laboratory microgrid. As a final remark, this article has shown that a virtual circuit breaker overcomes the

limitations of conventional circuit breakers by enhancing power quality and load supply.

REFERENCES

[1] V. Khadkikar, "Enhancing electric power quality using UPQC: A comprehensive overview," *IEEE Trans. Power Electron.*, vol. 27, no. 5, pp. 2284–2297, May 2012.

[2] B. Mirafzal and A. Adib, "On grid-interactive smart inverters: Features and advancements," *IEEE Access*, vol. 8, pp. 160526–160536, 2020.

[3] F. Nejabatkhah, Y. W. Li, and H. Tian, "Power quality control of smart hybrid ac/dc microgrids: An overview," *IEEE Access*, vol. 7, no. 9, pp. 52295–52318, 2019.

[4] M. Castilla, J. Miret, J. L. Sosa, J. Matas, and L. G. D. Vicuña, "Grid-fault control scheme for three-phase photovoltaic inverters with adjustable power quality characteristics," *IEEE Trans. Power Electron.*, vol. 25, no. 12, pp. 2930–2940, Dec. 2010.

[5] W. Alabri and D. Jayaweera, "Voltage regulation in unbalanced power distribution systems with residential PV systems," *Int. J. Elect. Power Energy Syst.*, vol. 131, Oct. 2021, Art. no. 107036.

[6] M. Khederzadeh and S. Zandi, "Enhancement of distribution system restoration capability in single/multiple faults by using microgrids as a resiliency resource," *IEEE Syst. J.*, vol. 13, no. 2, pp. 1796–1803, Jun. 2019.

[7] G. Liu, T. Jiang, T. B. Ollis, X. Li, F. Li, and K. Tomsovic, "Resilient distribution system leveraging distributed generation and microgrids: A review," *IET Energy Syst. Integr.*, vol. 2, pp. 289–304, 2020.

[8] M. Castilla, J. Miret, L. García de Vicuña, A. Borrell, and C. Alfaro, "Improving voltage imbalance in inverter-based islanded microgrids during line-to-line short circuits," *IET Power Electron.*, vol. 16, pp. 1889–1901, 2023.

[9] F. Nejabatkhah, Y. W. Li, and B. Wu, "Control strategies of three-phase distributed generation inverters for grid unbalanced voltage compensation," *IEEE Trans. Power Electron.*, vol. 31, no. 7, pp. 5228–5241, Jul. 2016.

[10] S. F. Zarei and M. Parniani, "A comprehensive digital protection scheme for low-voltage microgrids with inverter-based and conventional distributed generations," *IEEE Trans. Power Del.*, vol. 32, no. 1, pp. 441–452, Feb. 2017.

[11] A. H. Hajimiragha, M. R. Dadash Zadeh, and S. Moazeni, "Microgrids frequency control considerations within the framework of the optimal generation scheduling problem," *IEEE Trans. Smart Grid*, vol. 6, no. 2, pp. 534–547, Mar. 2015.

[12] M. H. Cintuglu, T. Ma, and O. A. Mohammed, "Protection of autonomous microgrids using agent-based distributed communication," *IEEE Trans. Power Del.*, vol. 32, no. 1, pp. 351–360, Feb. 2017.

[13] Y. Shang, S. Shi, and X. Dong, "Islanding detection based on asymmetric tripping of feeder circuit breaker in ungrounded power distribution system," *J. Mod. Power Syst. Clean Energy*, vol. 3, no. 4, pp. 526–532, Dec. 2015.

[14] S. Eberlein and K. Rudion, "Investigation of resynchronisation process and its influence on microgrid components," in *Proc. CIRED Workshop*, 2016, pp. 1–4.

[15] A. Vukojevic and S. Lukic, "Microgrid protection and control schemes for seamless transition to island and grid synchronization," *IEEE Trans. Smart Grid*, vol. 11, no. 4, pp. 2845–2855, Jul. 2020.

[16] D. Sharma, F. Sadeque, and B. Mirafzal, "Synchronization of inverters in grid forming mode," *IEEE Access*, vol. 10, pp. 41341–41351, 2022.

[17] S. Fahmy, Q. Walger, and M. Paolone, "Resynchronization of islanded unbalanced ADNs: Control, synchrocheck and experimental validation," *Elect. Power Syst. Res.*, vol. 211, Oct. 2022, Art. no. 108496.

[18] I. Ahmed et al., "Review on microgrids design and monitoring approaches for sustainable green energy networks," *Sci. Rep.*, vol. 13, Dec. 2023, Art. no. 21663.

[19] N. Hatziargyriou, "Microgrid protection," in *Microgrids: Architectures and Control*. Hoboken, NJ, USA: Wiley, 2014, pp. 117–164.

[20] B. Fani, G. Shahgholian, H. H. Alhelou, and P. Siano, "Inverter-based islanded microgrid: A review on technologies and control," *e-Prime, Adv. Elect. Eng., Electron. Energy*, vol. 2, 2022, Art. no. 100068.

[21] D. Hou, "Relay element performance during power system frequency excursions," in *Proc. 61st Annu. Conf. Protective Relay Engineers*, 2008, pp. 105–117.

[22] M. M. Eissa, "Current directional protection technique based on polarizing current," *Int. J. Elect. Power Energy Syst.*, vol. 44, no. 1, pp. 488–494, Jan. 2023.

[23] S. Vaca, A. Fonseca, F. Chapi, and F. Pérez-Yauli, "A new methodology for the analysis and optimal setting of directional polarisation methods for overcurrent elements in line protection applications," *IET Gener., Transmiss. Distrib.*, vol. 16, pp. 882–896, 2022.

[24] W. Chen et al., "Application of CS-MCT in dc solid state circuit breaker (SSCB)," in *Proc. IEEE 30th Int. Symp. Power Semicond. Devices ICs*, 2018, pp. 335–338.

[25] W. Li, Y. Wang, X. Wu, and X. Zhang, "A novel solid-state circuit breaker for on-board dc microgrid system," *IEEE Trans. Ind. Electron.*, vol. 66, no. 7, pp. 5715–5723, Jul. 2019.

[26] C. Liu et al., "A novel solid-state circuit breaker with robust breaking capability and high efficiency," *IEEE Trans. Power Electron.*, vol. 38, no. 10, pp. 13052–13063, Oct. 2023.

[27] L. Harnefors, "Modeling of three-phase dynamic systems using complex transfer functions and transfer matrices," *IEEE Trans. Ind. Electron.*, vol. 54, no. 4, pp. 2239–2248, Aug. 2007.

[28] X. Wang, L. Harnefors, and F. Blaabjerg, "Unified impedance model of grid-connected voltage-source converters," *IEEE Trans. Power Electron.*, vol. 33, no. 2, pp. 1775–1787, Feb. 2018.

[29] L. Harnefors, X. Wang, S. F. Chou, M. Bongiorno, M. Hinkkanen, and M. Routimo, "Asymmetric complex-vector models with application to VSC–grid interaction," *IEEE J. Emerg. Sel. Topics Power Electron.*, vol. 8, no. 2, pp. 1911–1921, Jun. 2020.

[30] H. Zhang, R. Liu, C. Xue, and Y. Li, "Active power enhancement control strategy of grid-forming inverters under asymmetrical grid faults," *IEEE Trans. Power Electron.*, vol. 39, no. 1, pp. 1447–1459, Jan. 2024.

[31] T. Liu and X. Wang, "Unified voltage control for grid-forming inverters," *IEEE Trans. Ind. Electron.*, vol. 71, no. 3, pp. 2578–2589, Mar. 2024.

[32] B. Fan et al., "A novel droop control strategy of reactive power sharing based on adaptive virtual impedance in microgrids," *IEEE Trans. Ind. Electron.*, vol. 69, no. 11, pp. 11335–11347, Nov. 2022.

[33] W. Cao, M. Han, X. Zhang, Y. Guan, J. M. Guerrero, and J. C. Vasquez, "An integrated synchronization and control strategy for parallel-operated inverters based on *V–I* droop characteristics," *IEEE Trans. Power Electron.*, vol. 37, no. 5, pp. 5373–5384, May 2022.

[34] M. Lu, "Virtual oscillator grid-forming inverters: State of the art, modeling, and stability," *IEEE Trans. Power Electron.*, vol. 37, no. 10, pp. 11579–11591, Oct. 2022.

[35] Z. Jin and X. Wang, "A *dq*-frame asymmetrical virtual impedance control for enhancing transient stability of grid-forming inverters," *IEEE Trans. Power Electron.*, vol. 37, no. 4, pp. 4535–4544, Apr. 2022.

[36] H. S. Das, S. Li, B. Lu, and J. Wang, "Virtual dynamic grid impedance and its impacts on harmonics and stability of inverter based resources plant," *IEEE Trans. Power Electron.*, vol. 37, no. 12, pp. 15469–15481, Dec. 2022.

[37] M. Li et al., "Unified modeling and analysis of dynamic power coupling for grid-forming converters," *IEEE Trans. Power Electron.*, vol. 37, no. 2, pp. 2321–2337, Feb. 2022.

[38] J. Duarte, M. Velasco, P. Martí, A. Borrell, and M. Castilla, "Remote multinodal voltage unbalance compensation in islanded ac microgrids," *IEEE Trans. Power Electron.*, vol. 39, no. 3, pp. 3052–3063, Mar. 2024.

[39] M. Castilla, M. Velasco, J. Miret, A. Borrell, and R. Ramón, "Control scheme for negative-sequence voltage compensation and current sharing in inverter-based grid-connected microgrids," *IEEE Trans. Power Electron.*, vol. 37, no. 6, pp. 6556–6567, Jun. 2022.

[40] A. Borrell, M. Velasco, A. Camacho, J. Miret, and M. Castilla, "Remote negative-sequence voltage fair compensation in grid-forming inverter-based islanded ac microgrids," *IEEE Trans. Power Electron.*, vol. 38, no. 10, pp. 12570–12582, Oct. 2023.

[41] J. M. Rey, M. Castilla, J. Miret, M. Velasco, P. Martí, and E. Mojica-Nava, "Negative-sequence voltage elimination for distributed generators in grid-feeding operation mode," *IET Power Electron.*, vol. 13, pp. 1764–1774, 2020.

[42] Y. Wang, J. Xu, L. Wang, and X. Guo, "A novel hybrid pulse train control strategy to mitigate voltage unbalance rate in stand-alone four-leg voltage source inverter system," *IEEE J. Emerg. Sel. Topics Power Electron.*, vol. 12, no. 2, pp. 2052–2066, Apr. 2024.

[43] L. M. Wedepohl and L. Jackson, "Modified nodal analysis: An essential addition to electrical circuit theory and analysis," *Eng. Sci. Educ. J.*, vol. 11, no. 3, pp. 84–92, Jun. 2002.

[44] A. G. Yepes, F. D. Freijedo, O. López, and J. Doval-Gandoy, "Analysis and design of resonant current controllers for voltage-source converters by means of Nyquist diagrams and sensitivity function," *IEEE Trans. Ind. Electron.*, vol. 58, no. 11, pp. 5231–5250, Nov. 2011.

[45] P. Rodríguez, A. Luna, R. S. Muñoz-Aguilar, I. Etxeberria-Otadui, R. Teodorescu, and F. Blaabjerg, "A stationary reference frame grid synchronization system for three-phase grid-connected power converters under adverse grid conditions," *IEEE Trans. Power Electron.*, vol. 27, no. 1, pp. 99–112, Jan. 2012.

[46] M. Castilla, J. Miret, A. Camacho, L. García de Vicuna, and J. Matas, "Modeling and design of voltage support control schemes for three-phase inverters operating under unbalanced grid conditions," *IEEE Trans. Power Electron.*, vol. 29, no. 11, pp. 6139–6150, Nov. 2014.

Mojtaba Ghodrati received the B.S. degree in electrical and electronic engineering and the M.Sc. degree in electrical and control engineering from the Islamic Azad University, Tehran, Iran, in 2006 and 2018, respectively. He is currently working toward the Ph.D. degree in electronic engineering with the Universitat Politècnica de Catalunya, Barcelona, Spain.

Since 2023, he has been a researcher on battery management systems with Centro Tecnológico de Automoción de Galicia, Pontevedra, Spain. His research interests include power electronics, microgrids, and battery management systems.

Ángel Borrell received the B.S. degree in electrical engineering, the M.S. degree in automation and industrial electronics engineering, and the Ph.D. degree in electronics engineering from the Technical University of Catalonia, Barcelona, Spain, in 1993, 2006, and 2012, respectively.

Since 1994, he has been an Associate Professor with the Department of Electrical Engineering, Escola Universitària Salesiana de Sarrià, Autonomous University of Barcelona, Barcelona, Spain, where he teaches courses on electrical machines and automation. His research interests include power electronics, electric motor drives, and renewable energy systems.

Miguel Castilla received the B.S., M.S., and Ph.D. degrees in telecommunication engineering from the Universitat Politècnica de Catalunya, Barcelona, Spain, in 1988, 1995, and 1998, respectively.

Since 2019, he has been a Full Professor with the Department of Electronic Engineering, Universitat Politècnica de Catalunya, where he teaches courses on the control of power electronics converters. His research interests include power electronics, control, renewable energy systems, and electrical microgrids.

Jaume Miret (Member, IEEE) received the B.S. degree in telecommunications and the M.S. and Ph.D. degrees in electronics engineering from the Universitat Politecnica de Catalunya, Barcelona, Spain, in 1992, 1999, and 2005, respectively.

From 1993 to 2011, he was an Assistant Professor with the Department of Electronic Engineering, Universitat Politecnica de Catalunya. Since 2011, he has been an Associate Professor with the Universitat Politecnica de Catalunya, where he teaches courses on digital design and circuit theory. His research interests include dc–ac converters, active power filters, and digital control.

Manel Velasco received the B.S. degree in maritime engineering and the Ph.D. degree in automatic control from the Technical University of Catalonia, Barcelona, Spain, in 1999 and 2006, respectively.

Since 2002, he has been an Assistant Professor with the Department of Automatic Control, Technical University of Catalonia. His research interests include artificial intelligence, real-time control systems, collaborative control systems, and microgrids.